J Mater Sci: Mater Electron **(2023) 34:1869**

Electrospun polyacrylonitrile (PAN)/polypyrrole (PPy) nanofiber-coated quartz crystal microbalance for sensing volatile organic compounds

Nesli Yagmurcukardes[1], Atike Ince Yardimci[2], Mehmet Yagmurcukardes[3], Inci Capan[4], Matem Erdogan[4], Rifat Capan[4], and Yaser Acikbas[1,*]

[1] *Department of Materials Science and Nanotechnology Engineering, Usak University, 1 Eylul Campus, 64200 Usak, Turkey*
[2] *Technology Transfer Office, Usak University, 64200 Usak, Turkey*
[3] *Department of Photonics, Izmir Institute of Technology, Izmir, Turkey*
[4] *Department of Physics, Faculty of Science, Balikesir University, 10145 Balikesir, Turkey*

Received: 17 June 2023
Accepted: 7 September 2023
Published online: 26 September 2023

ABSTRACT

In this study, electrospun polyacrylonitrile (PAN)/polypyrrole (PPy) nanofibers (NFs) coated quartz crystal microbalance (QCM) were investigated for their sensing characteristics against six different volatile organic compounds (VOCs): chloroform, dichloromethane, carbon tetrachloride, benzene, toluene and xylene. SEM, TEM, FT-IR and TGA analysis were carried out for the characterization of PAN/PPy nanofibers and characterization results of PAN/PPy NFs showed that these nanofibers were morphologically well-arranged and straightforward with a cylindrical shape with the average fiber diameter of 253.17 ± 27 nm. Among all the gas measurement tests, dichloromethane displayed the highest response values for PAN/PPy coated QCM sensors. When the reproducibility of kinetic studies for PAN/PPy NFs coated QCM sensors were examined, the most repetitive results were obtained by this QCM sensor during dichloromethane investigation and the diffusion coefficients of VOCs for the first and second regions increased with the order of xylene < toluene < benzene < carbontetrachloride < chloroform < dichloromethane. The sensitivities of the PAN/PPy nanofibers-coated QCM sensor against organic vapors are determined between 4.71 and 6.17 (Hz ppm^{-1}) × 10^{-4}. As a result, PAN/PPy nanofibers exhibited high sensitivity and selectivity for VOCs sensor applications, especially for dichloromethane.

1 Introduction

Due to the industrial developments such as motor vehicles, large combustion plant, solvents and petrol evaporation and personal needs, especially utilized in our homes such as building materials, paints, furniture, cleaning products, and cosmetics, amount of released pollutant gases and volatile organic compounds (VOCs) are increasing day by day. Studies showed that total solvent emissions are 30% higher

Address correspondence to E-mail: yaser.acikbas@usak.edu.tr

https://doi.org/10.1007/s10854-023-11281-1

than the estimated values and shows increasing trend with time [1]. In most cases VOCs are toxic and hazardous, thus, besides causing environmental risks such as greenhouse effect and air pollution, they lead to immune system problems such as headaches, sick building syndrome (SBS), lethargy, etc. [2–8]. Even though VOCs are known as produced in the outdoor environment by industrial waste gases, automobile exhausts, fuel combustions and photochemical pollutions; they take part in our indoor environments by decoration materials, cleaning agents, combustion of natural gases, smoking, etc. Therefore, it is necessary to develop ideal sensing materials in order to supply the increasing requirement for superior sensing performance.

Although abundant numbers of studies have published on the improvement and fabrication of the sensing materials, likely inorganic/organic semiconductors, organic conducting polymers received great attention due to their ability of working even at room temperature. Their outstanding physical and chemical properties make them essential candidate for low-cost, large-scale, lightweight and flexible sensing applications [9, 10]. Conducting polymers are also appropriate for surface modification and biocompatibility along large surface areas, therefore, they can easily be adapted into electronic and optoelectronic sensing devices [11, 12]. Since the early 1980s, polyaniline (PANI), polypyrrole (PPy), polythiophene (PTH) and polyacrilonitrile (PAN) have been the examples of conductive polymers used within gas sensors as active layers [13–18]. PPy is obtained by the polymerization of pyrrole, and thus it is a promising copolymer due to its easy synthesis and high conductivity. At first, it was used as components of electronic devices and chemical sensors. However, due to their easy modification, functionalization, and stability nowadays it is an attractive material for sensing industry. With the gas or vapour adsorption, PPy acts like p-type semiconductor and the interaction leads to alteration in conductivity [19–21]. The sensing capability of PPy may be improved depending on its functional groups [22]. PPy was first proposed as NH_3 sensor by when Nylander et al. in 1983 and rapid attention on polymer gas sensors has been achieved [23]. Lee et al. proposed an Au-polypyrrole nanorod as gas sensor for the detection of (VOC)s and they tested with three types of VOC gases (benzene, toluene, and acetic acid) over a wide concentration range from 10 to 100 ppm [24]. The highest sensitivity was achieved for acetic acid gas concentration. Kwon et al. constructed a PPy nanoparticle based chemiresistive sensor and used for the detection of acetonitrile, acetic acid, and methanol [25]. The sensor showed a minimum LOD which is close to 50 ppm of methanol. SnO_2 and ZnO decorated PPy nanocomposites oxides were used to detect ethanol and methanol, however, sensors didn't show high response as ammonia [26]. Additionally, as PPy is very fragile, it is important to support PPy with supporting composites. In literature, nanotubular PPy and nanofibrillar PANI sensors were compared for their detection performances for propanol, butanol, methanol, and ethanol alcohols [27]. Although both sensors detected the same minimum limit concentration of alcohols, PANI sensor showed higher responses with lower response time for all tested alcohols. Besides these results, the PPy sensor was recovered completely and showed a reversible which was not the case of the PANI sensor.

Electrospinning is a simple method that is used to produce various types of nanomaterials such as nanospheres and nanofibers (NFs). During the electrospinning process, the voltage is applied between the needle tip and the collector. At the same time an ejector causes polymer solution flow with a constant rate while the charges are collected at the surface of the solution. When the electrostatic repulsion exceeds the surface tension, the solution is ejected from a nozzle forming a jet. The fibers are formed during drying and homogenously deposited on the collector [28, 29]. The quality and the morphology of the nanostructures depend on several parameters such as the type of polymer, viscosity of the solution, applied voltage, distance between the tip and the collector etc. And various nanostructures for different purposes have been produced by electrospinning method. Therefore, to our knowledge, no study has been done to analyse the sensing ability of PAN/PPy NFs that are electrospun over quartz crystal microbalance (QCM) sensors with the aim of detecting dichloromethane, carbon tetrachloride, chloroform, m-xylene, benzene, and toluene as VOCs.

In our previous study PAN NFs coated over quartz crystals by electrospinning were investigated for sensing chloroform, dichloromethane and carbon tetrachloride [18]. Based on the abovementioned studies, we aimed to investigate sensing ability of PPy by using PAN as a supporting copolymer in order to prevent its fragile behaviour. In addition to this, PAN addition makes PPy usable in electrospinning process. To

our knowledge, no study has been done to analyse the sensing ability and the swelling dynamics' PAN/PPy NFs QCM chemical sensor. The first report of the interaction mechanisms between VOCs and PAN/PPy structure in terms of the binding energies of the molecules with PAN/PPy unit was also presented in this work. Constructed PAN/PPy nanofibrous sensors were been examined for sensing chloroform, dichloromethane, m-xylene, benzene, toluene and carbon tetrachloride VOCs. The performance of PAN/PPy nanofibrous sensor is comparable to the performance of PAN nanofibrous sensor [18] in terms of the diffusion coefficient values when these sensors expose to three different aliphatic hydrocarbons (dichloromethane, chloroform and carbon tetrachloride). The diffusion coefficient values of PAN/PPy nanofibrous sensor for both regions higher than PAN nanofibrous sensor's values for these saturated VOCs vapors.

2 Materials and methods

2.1 Materials

The Polyacrylonitrile (PAN) average molecular weight: 150,000 g·mol^{-1} and CAS number: 25014-41-9 was used as supporting copolymer. The polypyrrole (PPy) with conductivity > 0.005 S/cm and solvent N,N-dimethylformamide (DMF) was purchased from Merck Sigma-Aldrich to produce PAN/PPy electrospun NFs.

2.2 Fabrication of PAN/PPy nanofibers

In every electrospinning process, 8% weight ratio of PAN/PPy were first solubilized in 5 ml DMF to form electrospinning solutions. Initially, PAN was stirred about 1 h in DMF at 60 °C, and then PPy was inserted into the initial solution and mixed about 3 days at the same temperature to achieve the ultimate solution. PPy ratio in the total polymer was kept as 10 wt%. The developed solutions were stored into a 5 ml injector and exposed to15 kV voltage. Electrospinning system consists of 3 parts: syringe pump, power supply and collector. During this experiment, high voltage is applied to the polymer solution in the syringe from the power source via the electrode connected to the tip of the syringe. The applied voltage was kept at 15 kV, the distance between the collector and electrode was kept 25 cm and the flow rate of the solution was kept 1.5 µl/h. The electrospinning process was carried out at room temperature (20 °C). The Al foil was used to wrap collector and the electrospinning process completed in 2 h for each sample. QCMs were fixed on Al foil by sticking with tape and covered with PAN/PPy NFs during the electrospinning process. The illustration of the experimental system is presented in Fig. 1.

2.3 Characterization of the electrospun PAN/PPy NFs

Scanning electron microscopy (SEM, FEI QUANTA 250 FEG) and Transmission electron microscopy (TEM, FEI-Tecnai G2 F30) were utilized to analyse the morphology and the width of the PAN/PPy NFs were investigated from SEM images.

Fourier-Transform Infrared Spectroscopy (FT-IR, Perkin Elmer) was utilized for structural characterization of the PAN/PPy NFs to specify the types of chemical bonds and intermolecular interactions through nanofibers. FT-IR spectra were carried out with a scan range between 4000 and 450 cm^{-1}.

The thermal properties of PAN/PPy NFs were characterized by thermogravimetric analysis (TGA, Hitachi STA 7300) in the temperature range of 25–600 °C in the N_2 ambient at a heating rate of 10 °C /min.

2.4 QCM technique

Quartz crystal microbalance (QCM) platforms are preferable to be used for chemical sensors as they offer fast, simple handling, reliable and compact transducer elements. QCM measurements were carried with designed oscillating circuit for real-time detection that operating at desired temperature with the solid substrate of quartz crystal. The time dependent oscillating frequency was measured and stored through computer-controlled software system that is compatible with the quartz crystal. Using this system, the adsorption–desorption kinetics of VOCs through the thin film surface were recorded as a function of frequency shift. During the investigations, thin film coated sensors were subjected to periodic organic vapour exposures and the desorption of this molecules were ensured by the initiation of dry air. This procedure was carried out with the organic vapor introduced at four different concentrations, the volume of which is varied between 1.25 and 5 mL (25%, 50%, 75%, and 100%), into the gas cell. This measurement was repeated at least three cycles in order to monitor the repeatability of the fabricated sensor.

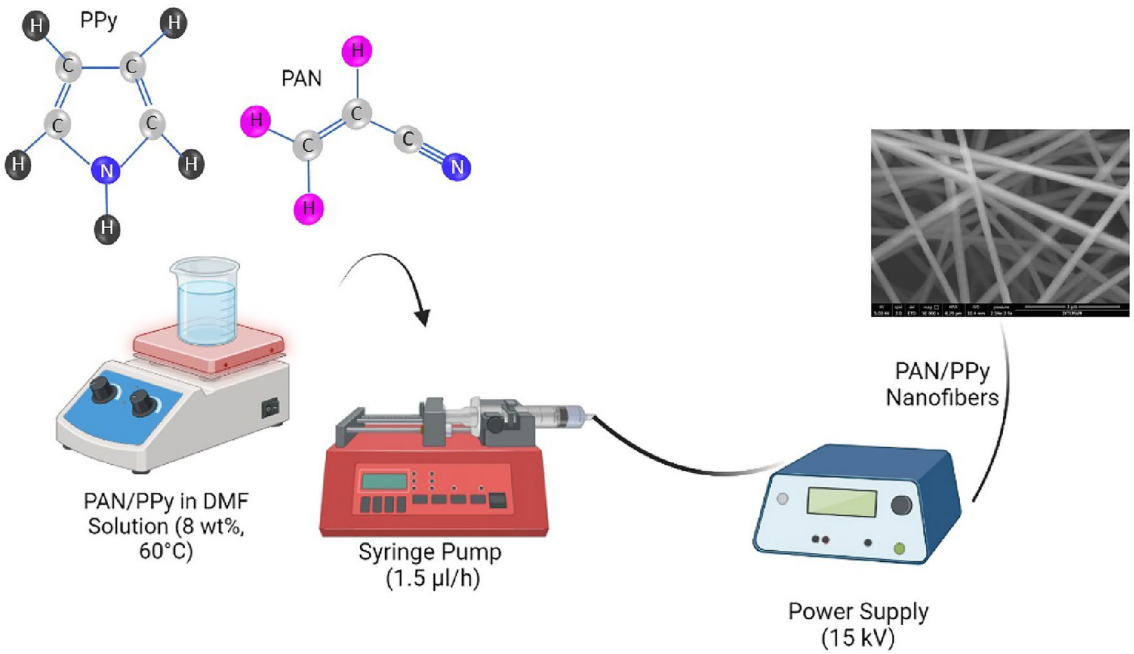

Fig. 1 The synthesis of PAN/PPy nanofibers by electrospinning method

2.5 Computational methodology

The binding energy calculations were considered to analyse the interaction between PAN/PPy polymers and selected VOCs by means of density functional theory (DFT) based ab-initio calculations. In order to describe the electron-exchange and correlation, the Perdew-Burke-Ernzerhof (PBE) [30] form of generalized gradient approximation (GGA) was adopted as implemented in the Vienna ab-initio simulation package (VASP) [31]. Regarding each ionic step, the convergence criterion for the total energy was set to 10^{-6} eV. In addition, the maximum force on each atom was chosen to be less than 10^{-5} eV $Å^{-1}$. The basics of DFT are summarized and presented in *Supplementary Material*.

3 Results and discussion

3.1 Morphological characterization results of the PAN/PPy NFs

In our previous study, PPy concentrations of 10, 25, and 50 wt% were tried to obtain beadless and regular PAN/PPy nanofibers and it was indicated that 10 wt% PPy was the appropriate concentration [32]. Therefore, in our study, PAN/PPy NFs containing 10 wt% PPy were chosen to investigate their sensing ability. The structure and the width values of electrospun PAN/PPy NFs were characterized by SEM. The SEM image displayed that as-grown PAN/PPy NFs were all morphologically well-arranged and straightforward with a cylindrical shape (Fig. 2.). Only a few beads were observed on the fibers. The average diameter of the PAN/PPy nanofibrous sample was measured as 253.17 ± 27 nm and the diameter distribution of the sample was given in Fig. 2d. In literature, the average fiber diameter for neat PAN nanofibers were measured as 290 nm [33], the decrease in fiber diameter with the addition of PPy resulted in increase in the solution conductivity which provides thinner nanofiber formation [34]. The TEM image showed that the nanofiber surface was not as smooth as it appeared in the SEM images, and the nanofibers were not hollow. The morphology, microstructure and size affect directly the sensing performance of gas sensor [35]. Nanofibers are considered to be very interesting for sensing applications with their large surface area, high charge carrier collection and transport in the axial orientation and the possibility of surface modification [36]. High surface area is suitable for the adsorption of target gases and allows rapid diffusion of gases species, thus increasing the sensor response. Besides, the nanoscale diameters of electrospun nanofibers offer many interesting properties such as excellent

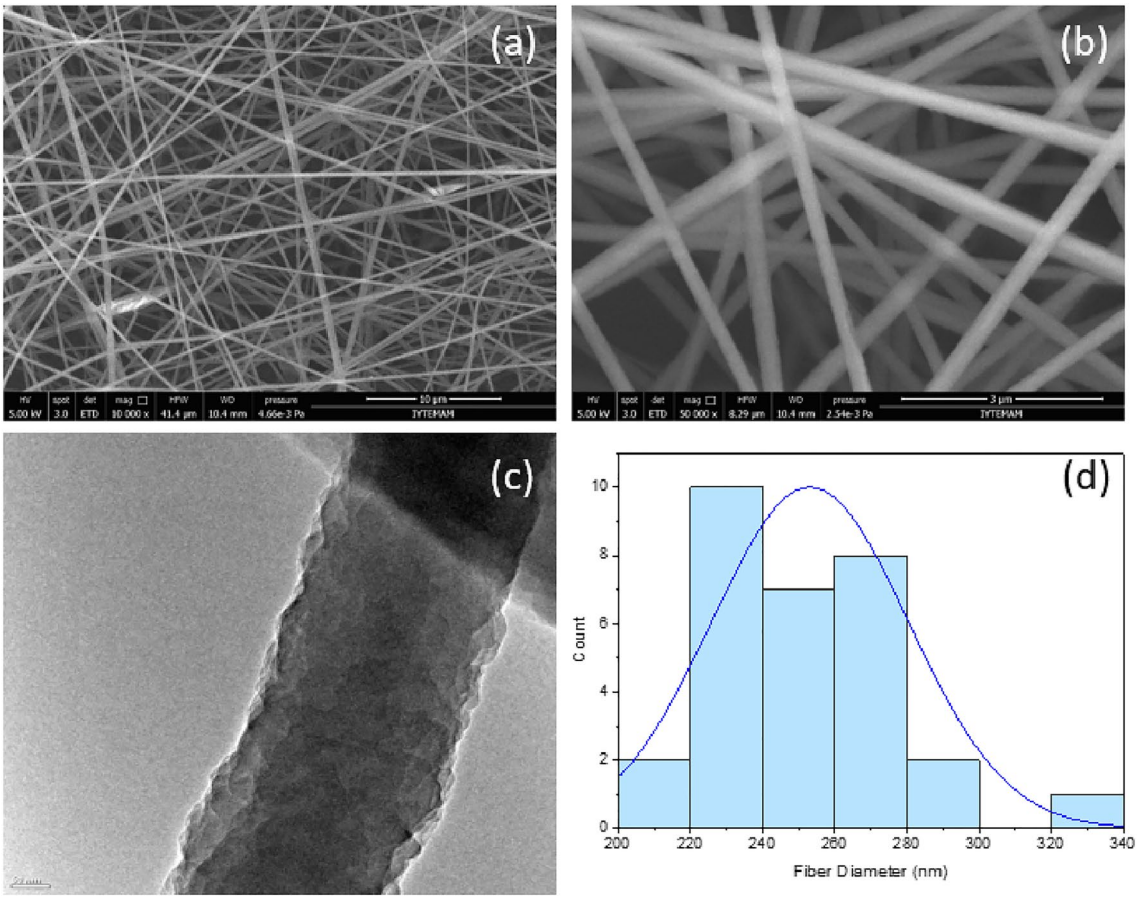

Fig. 2 SEM images of PAN/PPy NFs **a** 10.000, and **b** 50.000× magnifications. **c** TEM image of NFs **d** diameter distribution of NFs

flexibility in surface functionality and better mechanical properties compared to micro scale materials [38].

3.2 Structural and thermal characterization results of the PAN/PPy NFs

The structural properties of PAN/PPy NFs were analysed with FT-IR spectroscopy (Fig. 3.) The typical peak of PAN belongs to the C=C, –C≡N stretching at 1454, 2240 cm^{-1} were observed in the FT-IR spectra of the sample. The nitrile groups stretching at 2240 cm^{-1} [38, 39] originated from the existence of PAN and C–H stretching peaks at 2943 cm^{-1}, –C=O group stretching around 1735 cm^{-1}, and C=N stretching at 1667 cm^{-1} [40] were observed for PAN/PPy NFs. The peak at 1061 cm^{-1} corresponded to the C-H.

Based on the TGA graph of PAN/PPy NFs, firstly, the removal of water leading to the degradation step was observed in between the temperature interval of 70 and 120 °C. Degradation of pure PAN and pure PPy generate in two steps which start at about 310 and 500 °C for PAN and at about 210 and 410 °C for PPy [41]. PPy phase thermally degrades easier than PAN [42]. In our study, PAN/PPy NFs degradation occurred between 310 and 500 °C, the same as pure PAN due to the low concentration of PPy (Fig. 3). At 327 °C, TGA curve of nanofibers showed 63 wt% weight of the residue which was associated with cyclization of nitrile groups in PAN polymer chain. The second stage started at 327 °C and lasted at 460 °C with decomposition reaction of PAN and the char yield was about 40 wt%. On further heating at about 600 °C almost constant char yield of 36 wt% was observed [43].

3.3 PAN/PPy nanofibers coated-QCM Gas Measurements

In this study, the sensitivity of the PAN/PPy nanofibrous film coated QCM sensor to six different VOCs containing aliphatic and aromatic hydrocarbon groups was observed. Figure 4. Shows the PAN/PPy

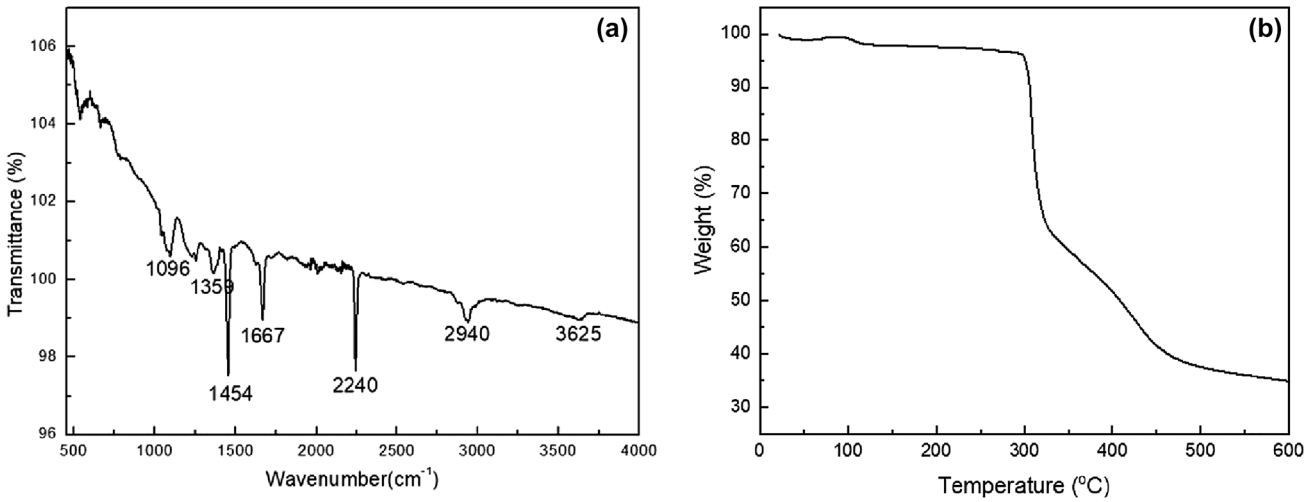

Fig. 3 FT-IR and TGA graphs of PAN/PPy NFs

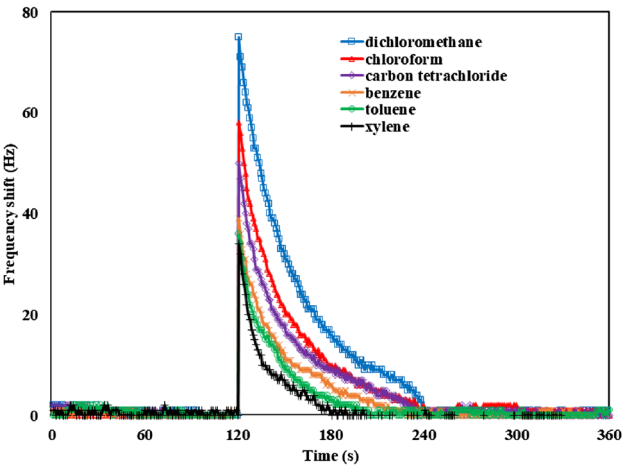

Fig. 4 The kinetic results of the PAN/PPy NFs-coated QCM sensor against to VOCs

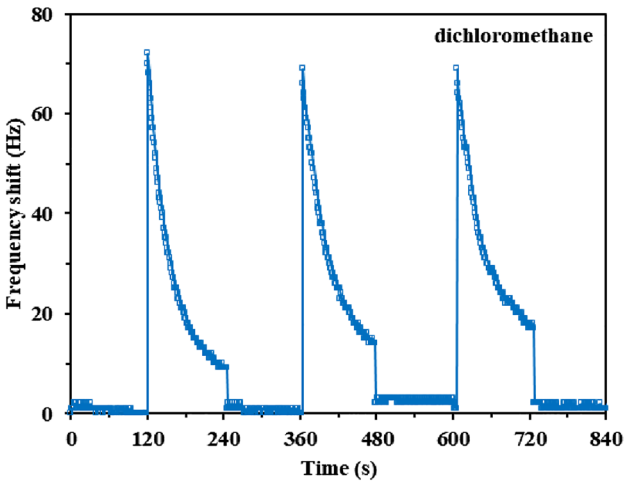

Fig. 5 Reproducibility of PAN/PPy nanofibers-coated chemical sensor for dichloromethane

nanofibrous film coated sensor exposed to dichloromethane, chloroform, carbon tetrachloride, benzene, toluene, and m-xylene as VOCs. Similar profiles were observed when VOCs were introduced into the the PAN/PPy NFs-coated QCM crystal. In the initial part, dry air was introduced into the gas cell for 120 s, and the variation of frequency along this time was found almost constant, till the VOC molecules are introduced into the experimental chamber forming the baseline of the PAN/PPy NFs-coated QCM sensor. Injection of gases into the gas cell initiates a surface alteration and accompanying diffusion process along the QCM sensor and the VOCs. The change in QCM frequency directly related with the amount of these reactions until the equilibrium state is reached. It has been observed that the values of frequency values were initially splashed for a few seconds and then decreased exponentially depending on time till the injection of dry air molecules into the chamber at 240 s. Consequently, the frequency values of the sensor returned to the initial baseline as a result of a reversible response of the PAN/PPy NFs-coated QCM sensor and thus, its recovery occurred for the following measurement.

For the PAN/PPy NFs coated QCM sensor, among all six detected vapours, dichloromethane showed the relatively high response values. Figure 5 displays the reproducibility of the PAN/PPy NFs coated QCM

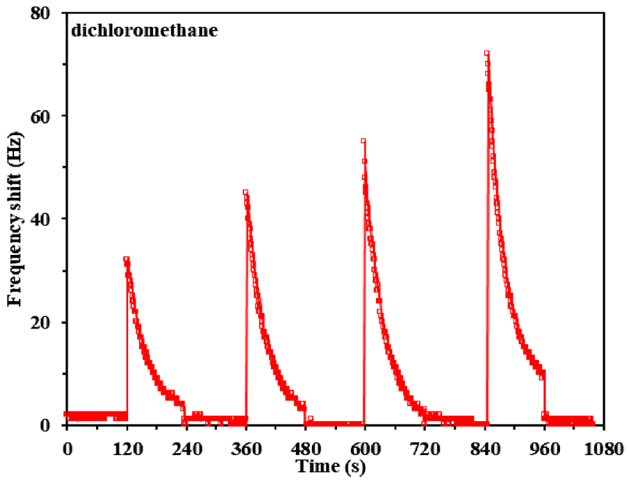

Fig. 6 The frequency changes of PAN/PPy nanofibers-coated chemical sensor for dichloromethane at different concentrations

sensor against dichloromethane. As a result of the reproducibility of kinetic studies for the mass sensitive sensor, it is obvious that the responses of PAN/PPy NFs-coated chemical sensor vapour are reproducible for dichloromethane. At the same time, the PAN/PPy nanofibers-coated chemical sensor is exposed to different concentrations of dichloromethane vapour and it is indicated that the frequency change increased with the increasing concentration as function of time (Fig. 6). The concentration values of organic vapor (see Table 1) in ppm are calculated by the formula as follows [44]:

$$c = \frac{\rho V\left(22.4\,Lmol^{-1}\right)10^{6}}{MV_0} \quad (1)$$

where c (ppm) is the concentration of vapor, ϱ (g cm^{-3}) is the density of vapor, V (mL) is the volume of vapor which is injected into the gas chamber, M (g mol^{-1}) is the vapor molecular weight, and V_0 is the volume of the gas chamber (~0.02 L). The vapor volume values are used in this study in the following order: 25% for V = 1.25 mL, 50% for V = 2.5 mL, 75% for V = 3.75 mL, and 100% for V = 5 mL

The sensitivity of PAN/PPy nanofibers coated-QCM sensor was obtained from the frequency shift curves when exposed to organic vapors in Fig. S1. The approximate curve was created from these frequency shifts. Frequency shifts versus concentrations of all organic vapors were obtained and given in Fig. S1. The sensitivities of the PAN/PPy nanofibers-coated chemical sensor against organic vapors are obtained for dichloromethane, chloroform, carbon tetrachloride, benzene, toluene and m-xylene, as 6.17, 5.75, 5.59, 4.96, 4.91, and 4.71 (Hz ppm^{-1}) × 10^{-4}, respectively. In this study, the rise time was defined as the time taken by the sensor to achieve 90% of the maximum frequency shift (Δf_{max}) in the case of gas adsorption [45, 46]. When surface adsorption effect took place, a sudden increase can be seen in Δf. Similarly, the decay time was defined as the time taken by the sensor response to reduce to 10% of its Δf_{max} value in the case of gas desorption. The values of the rise and the decay times for PAN/PPy NFs QCM chemical sensor against to all VOCs were determined using Fig. S2 and presented in Table 2.

3.4 The calculation of diffusion coefficients for organic vapours

In order to calculate the diffusion coefficient values of organic vapours at saturation concentration, Fick's

Table 1 The concentration values of organic vapors

Organic vapors	ρ (g cm^{-3})	M (g mol^{-1})	c (25%) × 10^3 ppm	c (50%) × 10^3 ppm	c (75%) × 10^3 ppm	c (100%) × 10^3 ppm
Dichloromethane	1.326	84.93	21.85	43.71	65.57	87.43
Chloroform	1.483	119.38	17.39	34.78	52.17	69.56
Carbon tetrachloride	1.594	153.82	14.47	28.94	43.41	57.88
Benzene	0.876	78.11	15.70	31.41	47.12	62.83
Toluene	0.870	92.14	13.21	26.43	39.65	52.87
m-xylene	0.869	106.16	11.46	22.93	34.40	45.87

Table 2 The values of the rise and the decay times

Organic vapor	$t_{response}$ (t_{rise}) (s)	$t_{recovery}$ (t_{decay}) (s)
Dichloromethane	0.88	91.5
Chloroform	0.92	85.4
Carbon tetrachloride	0.94	86.2
Benzene	0.89	92.2
Toluene	0.78	54.1
Xylene	0.75	42.5

second diffusion law [47] has been applied to clarify the swelling dynamics of the PAN/PPy NFs based QCM sensors.

In Fig. 4, the exponential decline of the response of PAN/PPy NFs coated QCM sensor between 120 and 240 s points out the initiation of the diffusion process with the entrance of vapour into the gas cell.

In Fig. 7, swelling cycles of the six types of VOCs were recorded for 120 s is presented with the plot of normalized reflective intensity versus diffusion time with the onset of t = 0. The diffusion coefficients (D) of VOCs could be derived by using the advanced Fick's diffusion equation from this data as expressed in the revealed section of the Supplementary Material.

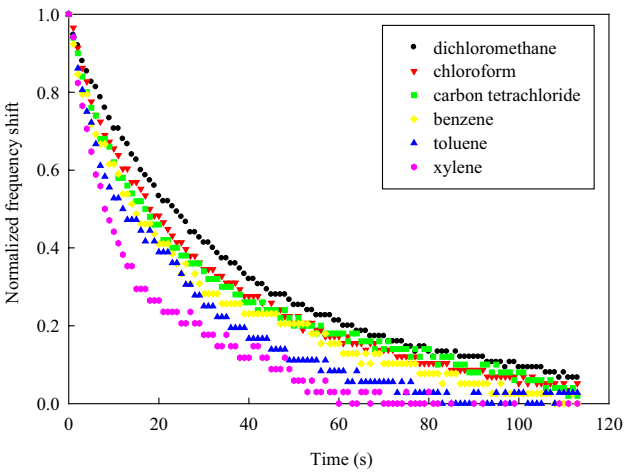

Fig. 7 The relation between the normalized kinetic response and swelling time for vapours

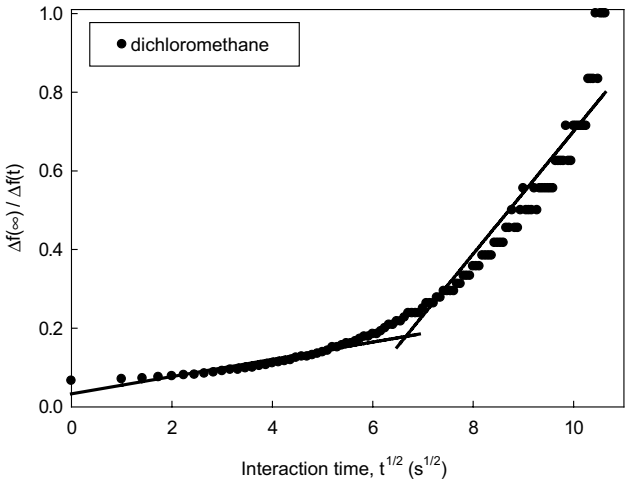

Fig. 8 The plot of the resonance frequency with the square root of the swelling time for dichloromethane

The plot of the correlation between the normalized frequency change and the square root of the swelling time for dichloromethane is shown in Fig. 8. The similar investigations were also carried for chloroform, carbon tetrachloride, benzene, toluene, xylene and all VOCs and presented in Figs. S3–S8, respectively.

If the slopes of the indicated linear regions are indicated, the swelling diffusion coefficients of the PAN/PPy NFs may be achieved. The obtained diffusion coefficient values of investigated vapours are lower in the second region when compared to initial cycle indicating the higher amount of diffusion occurring at the beginning of the swelling cycle that followed by reduction. The diffusion coefficient values of aliphatic and aromatic hydrocarbon groups are listed in Table 3 and graphed as a bar chart in Fig. 9.

3.5 Binding of VOCs to PAN/PPy molecules

In order to simulate the PAN/PPy structure, single unit molecule forming the PAN and that of PPy crystals were taken into account. The unoccupied orbitals of the C-atoms at the edges of the chain were saturated with H atoms. Firstly, we discuss the interaction mechanism between the PAN and PPy structures. It is shown that the PAN and PPy structures tend to interact weakly as the two layers bind via van der Waals (vdW) forces. The binding energy of PAN and PPy is calculated to be 484 meV indicating a physical interaction between the two structures (Fig. 10).

Table 3 The diffusion coefficients (D) calculated for first and second regions

Organic vapor	Molar volume ($cm^3\ mol^{-1}$)	Dipole moment (D)	$D(cm^2\ s^{-1})\times10^{-8}$ (first region)	$D(cm^2\ s^{-1})\times10^{-8}$ (second region)
Dichloromethane	64.10	1.60	72.0	10.09
Chloroform	80.70	1.08	69.2	7.67
Carbon tetrachloride	97.10	0	60.8	6.58
Benzene	86.36	0	56.3	6.21
Toluene	107.10	0.36	51.8	5.44
Xylene	122.00	0.30	43.2	4.77

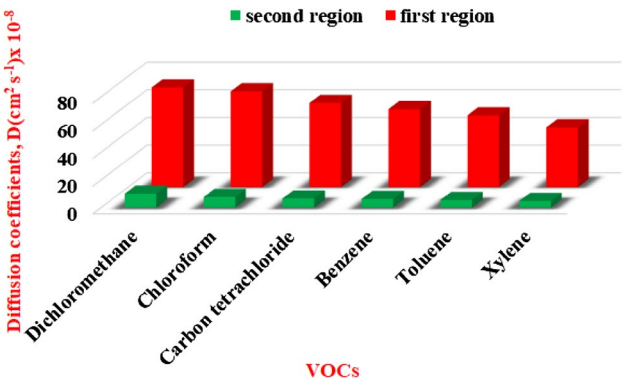

Fig. 9 The diffusion coefficients for all vapours

In order to understand the interaction mechanisms between VOCs, namely chloroform, dichloromethane, carbon tetrachloride, toluene, benzene, and xylene, and PAN/PPy structure are investigated in terms of the binding energies of the molecules with PAN/PPy unit. Our results reveal that all of the molecules are physically adsorbed on PAN/PPy either from PAN or from PPy sides. The calculated binding energies for each VOC molecule on both PAN and PPy side are presented in Fig. 11.

It is found that all of the VOCs prefer to interact with the PAN/PPy structure from PAN side except for the carbon tetrachloride which is adsorbed on the PPy side with a binding energy of 196 meV. Similar to the vdW type interaction between PAN and PPy, VOCs interact via weak vdW forces with the PAN/PPy structure with binding energies ranging from 196 to 335 meV. Among the Cl-based molecules, chloroform has the highest binding energy (334 meV) since of the bonds of C atom is saturated with H atom which interacts stronger with N atom of PAN as compared to that of Cl atom. By the similar argument that H atom of VOCs tends to interact from the N-site of PAN/PPy, the binding energies of toluene (335 meV), benzene (297 meV), and xylene (326 meV) are higher than those of dichloromethane (286 meV) and carbon tetra chloride (164 meV from PAN side).

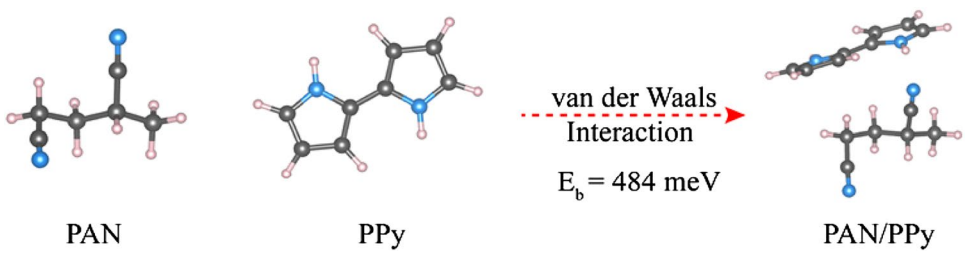

Fig. 10 Unit structures forming the PAN (on the left) and PPy (middle) crystals. The ground state structure for the PAN/PPy structure showing weak vdW interaction between them

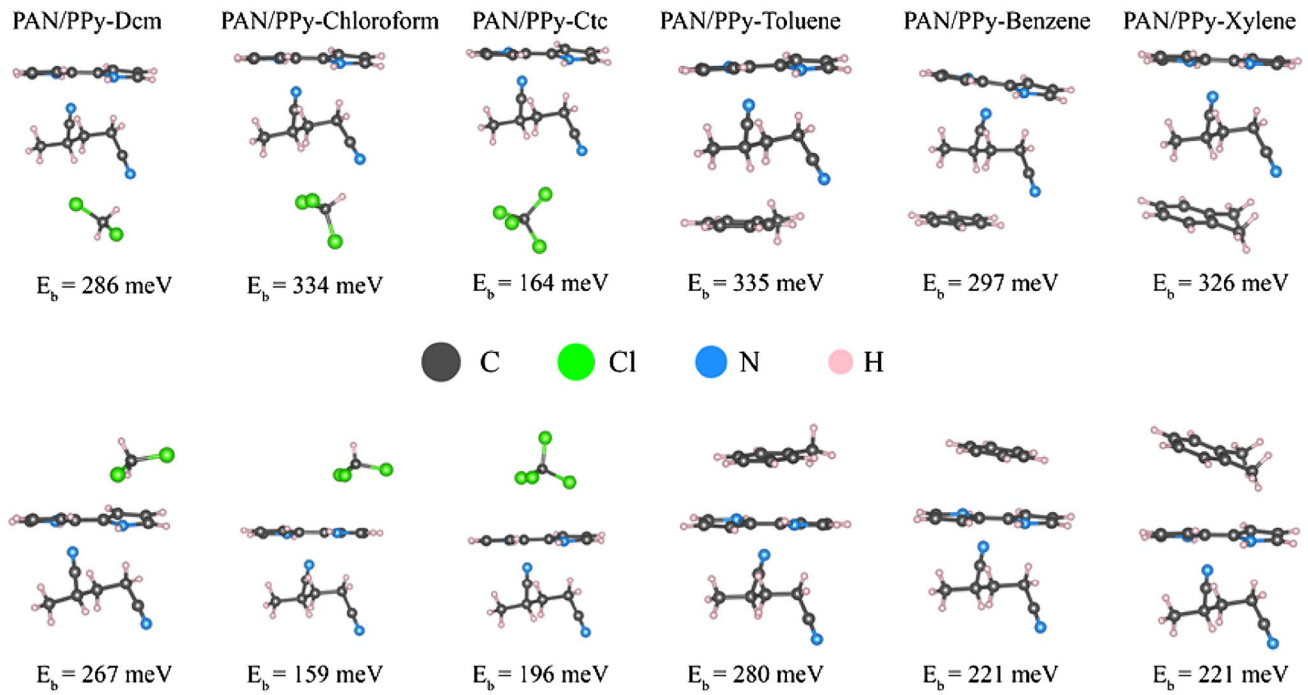

Fig. 11 The side views of the optimized VOC-PAN/PPy structures with the corresponding binding energies on the two sides, namely PAN and PPy sides

4 Conclusions

As a new sensing material, PAN/PPy nanofibers gas sensing properties for the chloroform, dichloromethane, carbon tetrachloride, benzene, toluene and xylene gases were investigated by QCM technique. PAN/PPy nanofibers were successfully deposited on the surface of QCM via electrospinning method.

For the PAN/PPy NFs coated QCM sensor, among the detected VOCs, dichloromethane displayed the highest response values, and these responses are reproducible. Among the six VOC molecules tested, the highest diffusion coefficient was obtained for dichloromethane with the value of 10.09×10^{-8} and 72.0×10^{-8} cm^2s^{-1} for the first and second regions, respectively. Overall, the PAN/PPy NFs coated QCM sensor exhibited excellent reversibility and potentially applied for dichloromethane detection.

Author contributions

NY, AIY, YA: Conceptualization, methodology, formal analysis, data curation, investigation, visualization, writing, and review. MY: Methodology, formal analysis, data curation, investigation, writing, and review IC, RC: Conceptualization, formal analysis, data curation, investigation, visualization, writing, and review. ME: Formal analysis, data curation, investigation, visualization, and review.

Funding

This present work was partially funded by The Scientific and Technological Research Council of Turkey (TUBITAK) (Project ID:118C477). The authors would like to thank TUBITAK for the financial supports given to the project.

Data availability

Data sharing is not applicable to this article as no datasets were generated or analysed during the current study.

Declarations

Conflict of interest The authors declare that they have no competing interests.

Supplementary Information The online version contains supplementary material available at https://doi.org/10.1007/s10854-023-11281-1.

References

1. J.K. Pearson, Atmos. Environ. (2019). https://doi.org/10.1016/j.atmosenv.2019.02.014
2. X. Kang, N. Deng, Z. Yan, Y. Pan, W. Sun, Y. Zhang, Mater. Sci. Semicond. (2022). https://doi.org/10.1016/j.mssp.2021.106246
3. W. Liu, R. Liu, X. Zhang, Appl. Surf. Sci. (2020). https://doi.org/10.1016/j.apsusc.2019.145174
4. S. Mo, Q. Zhang, J. Li, Y. Sun, Q. Ren, S. Zou, Q. Zhang, J. Lu, M. Fu, D. Mo, J. Wu, H. Huang, D. Ye, Appl. Catal. B Environ. (2020). https://doi.org/10.1016/j.apcatb.2019.118464
5. C.T. Yang, G. Miao, Y. Pi, Q. Xia, J. Wu, Z. Li, J. Xiao, Chem. Eng. J. (2019). https://doi.org/10.1016/j.cej.2019.03.232
6. X. Zhang, B. Gao, A.E. Creamer, C. Cao, Y. Li, J. Hazard. Mater. (2017). https://doi.org/10.1016/j.jhazmat.2017.05.013
7. T. Lin, X. Lv, Z. Hu, A. Xu, C. Feng, Sensors (2019). https://doi.org/10.3390/s19020233
8. A.H. Mamaghani, F. Haghighat, C. Lee, Appl. Catal. B (2017). https://doi.org/10.1016/j.apcatb.2016.10.037
9. C.S. Park, C. Lee, O.S. Kwon, Polymers **8**(7), 249 (2016)
10. D.N. Nguyen, H. Yoon, Polymers (2016). https://doi.org/10.3390/polym8040118
11. H. Yoon, Nanomaterials (2013). https://doi.org/10.3390/nano3030524
12. S.J. Park, O.S. Kwon, J.E. Lee, J. Jang, H. Yoon, Sensors (2014). https://doi.org/10.3390/s140203604
13. J.P. Cheng, J. Wang, Q.Q. Li, H.G. Liu, Y. Li, J. Ind. Eng. Chem. (2016). https://doi.org/10.1016/j.jiec.2016.08.008
14. L. Xue, W. Wang, Y. Guo, G. Liu, P. Wan, Sens. Actuators B Chem. (2017). https://doi.org/10.1016/j.snb.2016.12.064
15. Q. Zhong, H. Xu, H. Ding, L. Bai, Z. Mu, Z. Xie, Y. Zhao, Z. Gu, Colloids Surf. A (2013). https://doi.org/10.1016/j.colsurfa.2013.04.053
16. Y.C. Wong, B.C. Ang, A.S.M.A. Haseeb, A.A. Baharuddin, Y.H. Wong, J. Electrochem. Soc. (2019). https://doi.org/10.1149/2.0032003JES
17. L. Zhu, W. Zeng, Sens. Actuators B (2017). https://doi.org/10.1016/j.sna.2017.10.021
18. A. Ince Yardimci, N. Yagmurcukardes, M. Yagmurcukardes, I. Capan, M. Erdogan, R. Capan, O. Tarhan, Y. Acikbas, Appl. Phys. A Mater. Sci. Process. (2022). https://doi.org/10.1007/s00339-022-05314-5
19. M. Bazzaoui, J.I. Martins, E. Machnikova, E.A. Bazzaoui, L. Martins, Eur. Polym. J. (2007). https://doi.org/10.1016/j.eurpolymj.2007.01.013
20. N. Bhat, A.P. Gadre, V.A. Bambole, J. Appl. Polym. Sci. (2003). https://doi.org/10.1002/app.11641
21. C.W. Lin, Y.L. Liu, R. Thangamuthu, Sens. Actuators B (2003). https://doi.org/10.1016/S0925-4005(03)00323-X
22. M. Šetka, J. Drbohlavová, J. Hubálek, Sensors (2017). https://doi.org/10.3390/s17030562
23. T. Seiyama, Chemical sensors: *proceedings of the international meeting on chemical sensors*, Fukuoka, Japan, September 19–22, Elsevier. Chemical sensors. Tokyo (1983)
24. J.S. Lee, N.R. Yoon, B.H. Kang, S.W. Lee, S.A. Gopalan, S.W. Kim, S.H. Lee, D.H. Kwon, S.W. Kna, J. Nanosci. Nanotechnol. (2015). https://doi.org/10.1166/jnn.2015.11194
25. O.S. Kwon, J.Y. Hong, J.S. Park, Y. Jang, J. Jang, J. Phys. Chem. C (2010). https://doi.org/10.1021/jp1083086
26. M. Joulazadeh, A.H. Navarchian, Synth. Metal. (2015). https://doi.org/10.1016/j.synthmet.2015.10.026
27. M. Joulazadeh, A.H. Navarchian, IEEE Sens. (2014). https://doi.org/10.1109/JSEN.2014.2360915
28. J. Doshi, D. Reneker, J. Electrostat. (1995). https://doi.org/10.1016/0304-3886(95)00041-8
29. X. Li, X. Hao, H. Yu, H. Na, Mater. Lett. (2008). https://doi.org/10.1016/j.matlet.2007.08.003
30. J.P. Perdew, K. Burke, M. Ernzerhof, Phys. Rev. Lett. (1998). https://doi.org/10.1103/PhysRevLett.80.891
31. G. Kresse, J. Hafner, Phys. Rev. B (1993). https://doi.org/10.1016/0022-3093(95)00355-X
32. A. Ince Yardimci, H. Aypek, O. Ozturk, S. Yilmaz, E. Ozcivici, G. Mese, Y. Selamet, J. Biomim. Biomater. Biomed. Eng. (2019). https://doi.org/10.4028/www.scientific.net/JBBBE.41.69
33. A.C. Canalli Bortolassi, V.G. Guerra, M.L. Aguiar, L. Soussan, D. Cornu, P. Miele, M. Bechelany, Nanomaterials (2019). https://doi.org/10.3390/nano9121740
34. C.J. Angammana, S.H. Jayaram, IEEE Trans. Ind. Appl. (2011). https://doi.org/10.1109/TIA.2011.2127431
35. A. Mirzaei, V. Kumar, M. Bonyani, S.M. Majhi, J.H. Bang, J.Y. Kim, H.W. Kim, S.S. Kim, K.H. Kim, Asian J. Atmos. Environ. (2020). https://doi.org/10.5572/ajae.2020.14.2.85
36. A. Chinnappan, C. Baskar, S. Baskar, G. Ratheesh, S. Ramakrishna, J. Mater. Chem. C. (2017). https://doi.org/10.1039/C7TC03058D
37. M. Yanılmaz, A.S. Sarac, Text. Res. J. (2014). https://doi.org/10.1177/0040517513495943

38. F. Yalcinkaya, B. Yalcinkaya, A. Pazourek, J. Mullerova, M. Stuchlik, J. Maryska, Int. J. Polym. Sci. (2016). https://doi.org/10.1155/2016/4671658
39. W. Zheng, Z. Li, T. Sun, X. Ruan, Y. Dai, X. Li, C. Zhang, G. He, J. Membr. Sci. (2022). https://doi.org/10.1016/j.memsci.2022.120330
40. L. Chen, L. Bromberg, H. Schreuder-Gibson, J. Walker, T.A. Hatton, G.C. Rutledge, J. Mater. Chem. (2009). https://doi.org/10.1039/B818639A
41. L. Ji, Y. Yao, O. Toprakci, Z. Lin, Y. Liang, Q. Shi, A.J. Medford, C.R. Millns, X. Zhang, J. Power. Sour. (2010). https://doi.org/10.1016/j.jpowsour.2009.10.021
42. C. Luo, J. Wang, P. Jia, Y. Liu, J. An, B. Cao, K. Pan, Chem. Eng. J. (2015). https://doi.org/10.1016/j.cej.2014.09.116
43. H.P. Karki, L. Kafle, D.P. Ojha, J.H. Song, H.J. Kim, Sep. Purif. Technol. (2019). https://doi.org/10.1016/j.seppur.2018.08.053
44. Y. Acikbas, M. Erdogan, R. Capan, F. Yukruk, Sens. Actuators B: Chem. (2014). https://doi.org/10.1016/j.snb.2014.04.051
45. K.S. Eu, K.M. Yap, Int. J. Adv. Robot. Syst. (2018). https://doi.org/10.1177/1729881418755877
46. J. Gonzalez-Jimenez, J.G. Monroy, J.L. Blanco, Sensors (2011). https://doi.org/10.3390/s110606145
47. J. Crank, *The mathematics of diffusion* (Oxford University Press, New York, 1975)